(Received 2 March 2025, Accepted 14 May 2025, Scheduled 22 June 2025)

A MIMO Antenna for 5G Wireless Applications, Designed with Hybrid Fractal Geometry and Incorporating CSRR Loading

Amandeep Kaur[1,*] and Jagtar S. Sivia[2]

[1] Department of Electronics and Communication Engineering, Punjabi University, Patiala, Punjab 147002, India
[2] YDoE, Punjabi University Guru Kashi Campus, Talwandi Sabo, Bathinda, Punjab 151302, India

ABSTRACT: This paper demonstrates a Hybrid Fractal MIMO Antenna (HFMA) integrated with a Complementary Split Ring Resonator (CSRR) for fifth-generation wireless applications. Two radiating elements based on Meander and Minkowski Hybrid fractal geometry are included in the proposed design. The defected ground plane, along with CSRR, has been employed to enhance the isolation, bandwidth, gain, and other performance characteristics of the proposed HFMA. The proposed antenna was constructed using Rogers RT/duroid 5880 material. The designed model offers a maximum isolation of −55.86 dB and a wide bandwidth of 28.72 GHz, in the frequency range from 1.28 GHz to 30 GHz. All the diversity parameters of the designed antenna are found within operating limits. The proposed antenna is capable of covering multiple 5G spectrum bands, including LTE band 46 (5.15–5.925 GHz), 5G New Radio and 3.5 GHz frequency bands (3.3–5.0 GHz), the 26 GHz 5G spectrum, the European Union 5G spectrum (5.9–6.4 GHz), and is highly suitable for a range of other advanced applications, including Internet of Things (IoT), satellite communications, and vehicular networks in the frequency range of 1–30 GHz band.

1. INTRODUCTION

In recent times, the need for wireless communication with high channel capacity, rapid data transfer rates, and a decent level of reliability in transmission has become increasingly important. However, Single-Input Single-Output (SISO) antennas cannot perform these functions due to their limited channel capacity. Research efforts by different researchers have resulted in the technology development in Multiple-Input Multiple-Output (MIMO) communication, which allows data to be transmitted at high rates in densely populated areas without using more power or spectrum [1]. Nowadays, 5G communication networks are commonly employed in mobile devices due to their higher data transfer rate and shorter delays than the current 4G systems. Currently, the foundation of 5G wireless systems is MIMO antenna technology, which offers high data rates within constrained bandwidth and power levels [2]. In a multipath environment, several antenna systems were formerly employed to increase the number of individual channels. In portable handheld devices due to limited space allocation, there is often very little space between elements, resulting in mutual coupling and performance degradation [3]. Many strategies have been used in the literature to decrease mutual coupling and increase isolation without compromising the presentation terms including electromagnetic band gap (EBG) arrangement, ground structures with defects [4], utilizing metamaterials [1], using dielectric resonators [5] incorporating parasitic elements [6], using Substrate Integrated Waveguide (SIW), slots, slits, and stubs on the radiating elements and in the ground [7], and incorporating SRR [8] and CSRR [9]. Furthermore, several hybrid fractal shapes were employed in the construction of the patch of the suggested antenna, including [10], in which Kaur and Sivia used firefly algorithm along with an artificial neural network to design a novel antenna for biomedical applications. The compact hybrid fractal antenna proposed by Bangi and Sivia is based on Minkowski and Hilbert Curves for wireless applications [11]. Furthermore, eight elements-based fractal arrays have been designed by Bhatia and Sivia for multiband applications [12]. A wearable hybrid fractal antenna that utilizes Koch and Meander curves using Particle Swarm Optimization (PSO) was further presented by Sran and Sivia [13]. Further, a novel meander fractal star-like wearable fractal antenna is designed by Sran and Sivia [14]. By hybridizing Minkowski fractal curves with hexagonal radiating patches, the wideband antenna has been designed by Bharti and Sivia [15]. A circular-type hybrid fractal antenna with defected ground plane (DGP) along with the artificial bee colony (ABC) algorithm was addressed by Kaur and Sivia [16]. Then, Kakkar et al. designed an I-shaped fractal antenna with optimal performance for emergency management wireless communication [17]. An ultra-wideband monopole antenna design using a lantern was presented by Kaur et al. [18]. A wide variety of fractal antennas have been developed utilizing fractal and hybrid fractal geometries suitable for 5G communication. MIMO antennas are an ideal choice for integrally justifying network quantity and multipath, providing a high degree of link reliability, channel volume, and gain exposure, which are essential for illustrating MIMO's quantity and spectrum efficiency. Researchers have worked on this track to design enormous MIMO antenna structures that are appropriate for 5G networks [19–23]. Table 1 presents the comparative analysis of several previously designed antennas.

* Corresponding author: Amandeep Kaur (sidhu.amandeep23@gmail.com).

TABLE 1. Comparative analysis of several earlier developed antennas in the literature.

Ref.No.	Size (mm^2)	Antenna Type	Bandwidth (GHz)	Gain (dB/dBi)	Remarks
[4]	8.6×17	Printed Patch Array	-	10.53 dB	Compact size but small bandwidth
[6]	72×72	UWB MIMO	10.5	6 dBi	Wideband but large area
[7]	65×20	Triple Band MIMO	-	3.28 dBi	Nearly omni-directional radiation pattern but moderate radiation gain
[8]	60×57	Planar Multiple Antenna	0.45	2.57 dBi	Good isolation but small bandwidth
[9]	100×50	MIMO	0.05	-0.8 dBi	Good isolation but small gain and bandwidth
[10]	26×21	Giuseppe Peano and Cantor set HFA	0.48	10.19 dB	Compact size but covers small band
[11]	50×37	Minkowski and Hilbert Curves Based HFA	-	12.2 dB	Better gain but narrow band coverage
[13]	58×52	Wearable Hybrid Fractal Antenna	0.31	8.55 dB	Moderate gain and bandwidth
[15]	24×30	Minkowski fractal curves HFA	10.86	4.54 dB	Good bandwidth with moderate gain
[17]	26.25×26.25	Fractal shaped Metasurface Antenna	0.2	1.56 dBi	Compact size with small gain
[20]	5.5×5.16	Microstrip Patch MIMO Antenna	1.95	6.14 dBi	Compact size but covers small band
[22]	75.7×42.9	MIMO antenna array	-	-	High gain but low isolation
[24]	72×72	UWB MIMO antenna	10.5	6 dBi	Large size with moderate gain

The literature analysis also highlights a gap: despite extensive study into different MIMO antenna configurations, a specialized hybrid fractal MIMO antenna tailored for 5G has not yet been designed. In order to satisfy the dynamic frequency and performance needs of 5G and beyond, this suggests a promising area for innovation where new combinations of fractal geometries should be further explored.

Based on an extensive literature review in order to address the research gap, in this paper, Meander and Minkowski curves-based hybrid fractal MIMO antenna loaded with CSRR is designed for 5G wireless applications. The proposed design exhibits a wide range of impedance bandwidth of 28.72 GHz (1.28–30 GHz). The suggested antenna is designed and simulated using the ANSYS HFSS software. A comparison is made between the results of the proposed design with and without CSRR, and it is found that CSRR-loaded antennas have better isolation, bandwidth, mutual coupling, and gain. The designing procedure of dual-port hybrid fractal MIMO antenna loaded with CSRR along with simulated and fabricated results is presented in the following segments.

2. DESIGN METHODOLOGY AND ANALYSIS OF MIMO ANTENNA

This manuscript proposes and examines a hybrid Minkowski and Meander fractal curves based half-octagonal MIMO antenna with two ports in two distinct stages. To optimize its parameters regarding S_{11} and bandwidth (BW), it starts with the initial design and adjustment of a single unit element. In the final stage, a single element's design is duplicated in opposite directions. The detailed discussion of the aforementioned antenna design steps is discussed in the subsequent subsections. The two-port CSRR-loaded hybrid fractal-shaped MIMO antenna has been proposed and examined in this manuscript.

First and foremost, the design of the proposed MIMO antenna starts with the design of an octagon-shaped radiating patch as depicted in Fig. 1 as step-1, and consists of different steps as illustrated in Fig. 1. The radius P_1 of the octagon-shaped patch has been evaluated using Equation (1) by utilizing numerous manipulative parameters such as the height of the substrate (h) relative permittivity of the substrate (ε_r), and resonant frequency (f_r). By using different relative parameters, the evaluated value of radius P_1 has been obtained and found to be 14.85.

$$P_1 = \frac{F}{\left\{1 + \frac{2h}{\pi F \varepsilon_r}\left[\ln\left(\frac{\pi F}{2h}\right) + 1.7726\right]\right\}^{\frac{1}{2}}} \tag{1}$$

where $F = \frac{8.791 \times 10^9}{f_r \sqrt{\varepsilon_r}}$.

A Rogers RT/duroid 5880 substrate is used to construct the proposed antenna design having dimensions of 75 mm $\times$ 45 mm

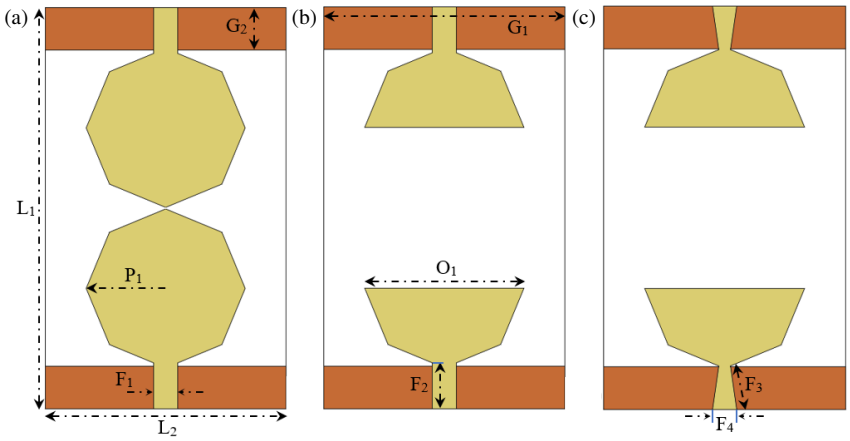

FIGURE 1. Designing steps of HFMA; (a) step-1, (b) step-2 (simple feed) and (c) step-3 (tapered feed).

along with a dielectric constant of 2.2 and a thickness of 1.6 mm. A transmission line feed of 50 Ω has been applied after the designing of two octagonal-shaped patches. To improve impedance matching, the partial ground plane with length "G_2", as shown in Fig. 1(a) named step-1, has been applied to these patches over the desired frequency range. Further, improved impedance matching has been achieved by etching half-octagonal patches as shown in Fig. 1(b). Then as shown in Fig. 1(c), the transmission line has been tapered in step-3 to improve impedance matching based on the reflection coefficient.

The various design steps for proposed dual-element HFMA have been elaborated in Fig. 1. This approach mainly consists of three phases of designing from step-1 to step-3. In Fig. 2, the different S-parameters are compared for each step.

From Fig. 2, it can be seen that the antenna taken into consideration in the first step (step-1) radiates between S_{11} values ranging from −10 dB to −36.81 dB for three frequency bands of 1.61–10.83, 17.30–23.40, and 24.35–30.00 GHz with corresponding BWs of 9.22, 6.10, and 5.65 GHz and maintain the isolation (S_{21}) of −17.63/−37.02/−29.50/−31.74 dB. Fig. 2 shows that the proposed antenna's performance is improved. This improvement is due to the etching of a half-octagonal patch, as outlined in step-1, resulting in enhanced isolation and an increased number of peak resonant frequency bands. Additionally, at step-3, the antenna features a wider bandwidth of 27.42 GHz from 2.58 to 30 GHz because of a tapered feed line

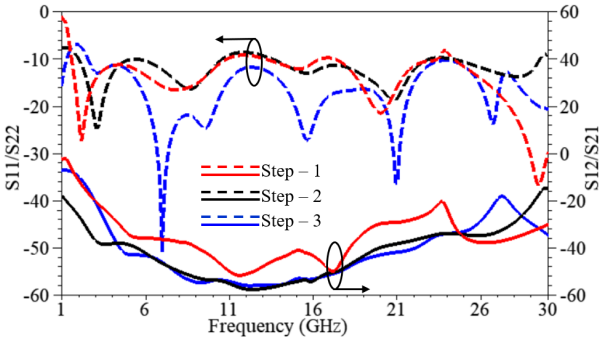

FIGURE 2. Comparison of reflection coefficient and isolation plot of different steps of designed HFMA.

as compared to the preceding step. Moreover, the antenna configuration at step-3 demonstrates additional frequency bands along with enhanced reflection coefficient and isolation. Table 2 lists all the results of the various design processes involved in the proposed HFMA. As explained above, the performance is improved in terms of isolation, impedance bandwidth, and reflection coefficient by altering the shape of the proposed design. Moreover, by altering the antenna's shape, the primary goal of this effort to construct a wideband antenna with a broader bandwidth has been accomplished.

3. HYBRID GEOMETRY OF PROPOSED DESIGN

By merging two or more distinct fractal geometries, hybrid fractal antennas can be developed. The structure of the proposed design combines Minkowski and Meander fractal shapes in a hybrid manner. The proposed MIMO antenna geometry is based on the hybrid combination of Meander and Minkowski fractal geometries. The fractal antenna has the capability to exhibit miniaturization along with wideband characteristics. The Meander curve improves the impedance bandwidth, and the Minkowski fractal curve contributes to the multiband nature of an antenna, so these two geometries are hybridized and superimposed on the semi-octagon-shaped radiating patch to generate the novel geometry of the antenna. The proposed hybrid fractal MIMO antenna depicts the wide band behavior of 28.72 GHz (1.28 to 30.0 GHz). Hence by combining these two geometries, multiband and wideband behavior is obtained. Additionally, the incorporation of CSRR and defective ground plane enhances isolation, bandwidth, gain, and other performance characteristics of the proposed HFMA. So hybrid fractal geometry was chosen over other methods.

The steps for hybridization of these curves are shown in Fig. 3. At the start, the straight line as depicted in Fig. 3(d) is called an initiator ($n = 0$), and the hybrid combination of Meander and Minkowski is used as a generator curve ($n = 1$). To obtain the second iteration of the suggested shape, each straight segment of the generator is also substituted with itself, according to Fig. 3(f). The proposed curve used for the HFMA antenna is generated as listed in Fig. 3(f). Using the following formula,

TABLE 2. Comparison of results for various design steps of HFMA.

Design steps	Resonant frequency range (GHz)		Peak resonant frequency bands (GHz)	Reflection coefficient (S_{11}/S_{22}) dB	Isolation (S_{12}/S_{21}) dB	Bandwidth (GHz)
	F_L	F_U				
Step-1	1.61	10.83	2.7/7.8/ 20.10/29.40	−27.42/−16.60/ −21.42/−36.81	−17.63/−37.02/ −29.50/−31.74	9.22
	17.30	23.40				6.10
	24.35	30.00				5.65
Step-2	2.02	10.60	3.10/8.7/15.7/ 20.80/28.30	−24.92/−16.39/−13.08/ −18.91/−13.74	−37.19/−51.61/−53.91/ −38.34/−27.13	8.58
	13.50	22.90				8.50
	24.20	29.50				5.30
Step-3	2.58	30.00	3.10/7.0/9.60/ 15.6/21.0/26.70	−12.98/−50.76/−24.70/ −27.24/−36.26/−23.85	−21.53/−45.85/−54.41/ −53.16/−41.69/−21.95	27.42

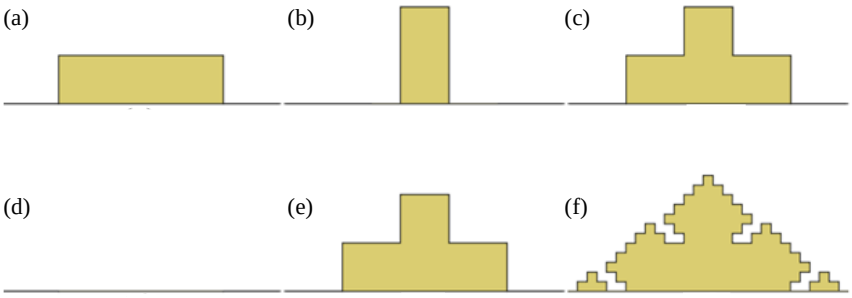

FIGURE 3. Generation of Meander-Minkowski hybrid curve; (a) Minkowski, (b) Meander, (c) hybrid curve, (d) initiator, (e) generator, and (f) proposed Meander-Minkowski hybrid fractal geometry.

the curve's total length (L) has been calculated.

$$L = h\left(\frac{N}{P}\right)^{n} = 29.69\left(\frac{9}{5}\right)^{2} = 96.19\,\text{mm} \tag{2}$$

There are N segments in the curve; h is its height; P represents fragments; and n is the number of repetitions. In addition, the self-similarity fractal index (D) was computed using the subsequent formula:

$$D = \frac{\log(N)}{\log(P)} = \frac{\log(9)}{\log(5)} = 1.36 \tag{3}$$

IFS function has been utilized for the generation of a hybrid structure for the proposed design, which has not been elaborated here for the sake of simplicity.

Further, this hybrid geometry is incorporated on both ports of the antenna designed as shown in Fig. 1 (step-3). The resultant antenna is obtained as shown in Fig. 4(a). Further, for better outcomes, a CSRR is incorporated in the proposed design as depicted in the following section.

4. DESIGN AND ANALYSIS OF CSRR

As discussed in the above section, a hybrid combination of Meander and Minkowski geometries was obtained as shown in Fig. 4(a). It has been demonstrated in the previous section that as in Fig. 1 (step-3), the proposed HFMA reports wider bandwidth and better impedance characteristics than the antenna constructed in Fig. 1 (steps-1 & -2). Now, as shown in Fig. 4(b), the performance of the suggested HFMA is improved in this portion by etching CSRR in the patch of the proposed design. As seen in Fig. 4(b), a constructed CSRR is composed of two concentric elliptical slots with distinct radii and identical gaps and widths. To achieve wide-band operation, the ring thickness has been appropriately varied and optimized. The designed CSRR-loaded prototype model is shown in Fig. 4(b). Parametric dimensions of the proposed wideband CSRR-loaded HFMA are depicted in Table 3.

The loading of CSRR enhances isolation, bandwidth, gain, and other performance characteristics of the proposed HFMA. A comparison is also made between the results of the proposed design with and without CSRR, and it is found that CSRR-loaded antennas have better isolation, bandwidth, mutual coupling, and gain.

5. RESULTS AND DISCUSSIONS

The comparative plot of reflection coefficient and isolation versus frequency is shown in Fig. 5. From the plot it has been

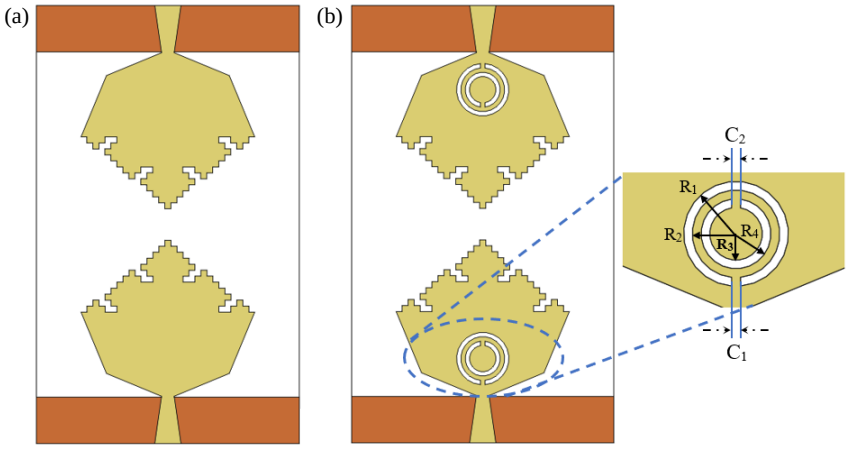

FIGURE 4. Proposed HFMA; (a) without CSRR and (b) with CSRR.

TABLE 3. Parametric dimensions of proposed wideband CSRR loaded HFMA.

Parameters	Dimensions (mm)	Parameters	Dimensions (mm)	Parameters	Dimensions (mm)
L_1	75.0	F_1	4.50	R_1	4.5
L_2	45.0	F_2	8.10	R_2	3.75
P_1	14.85	F_3	8.18	R_3	3.0
G_1	45.0	F_4	4.50	R_4	2.25
G_2	7.95	C_1	0.75		
O_1	29.69	C_2	0.75		

TABLE 4. Comparison of results for HFMA with and without CSRR.

Hybrid MIMO antenna	Resonant frequency range (GHz)		Peak resonant frequency bands (GHz)	Reflection coefficient (S_{11}/S_{22}) dB	Isolation (S_{12}/S_{21}) dB	Bandwidth (GHz)
	F_L	F_U				
without CSRR	2.89	23.00	3.4/7.0/9.6/ 15.6/20.80/27.90	−44.64/−12.21/−21.93/ −20.39/−36.50/−17.50	−8.63/−38.54/−60.15/ −55.82/−42.30/−28.42	20.11
	24.00	30.00				6.00
with CSRR (Proposed antenna)	1.28	30.00	2.3/7.2/9.10/ 15.50/21.30/23.80	−12.99/−32.49/−23.47/ −19.49/−45.58/−17.59	−24.72/−33.27/−49.97/ −55.86/−44.07/−19.25	28.72

analyzed that by incorporating CSRR, the proposed design exhibits a wider bandwidth of 28.72 GHz in the frequency range from 1.28 GHz to 30.00 GHz than the antenna without CSRR. Additionally, the performance of the proposed antenna is also enhanced with regard to reflection coefficient, and maximum isolation −55.86 dB was obtained. The comparison of the proposed HFMA with and without CSRR is also shown in Table 4 for additional clarity.

5.1. Surface Current Distribution

A surface current density analysis was done to investigate the antenna parts that mainly affect radiation patterns and coupling between the MIMO elements. Using surface current distribution plots at different frequencies such as 2.3, 7.2, 9.10, 15.50, 21.30, and 23.80 GHz, the effects of embedding CSRR are analyzed as shown in Fig. 6. In the proposed two-port antenna, one port must be terminated with a matching load of 50 Ω and the other excited simultaneously. Fig. 6 clearly shows the higher

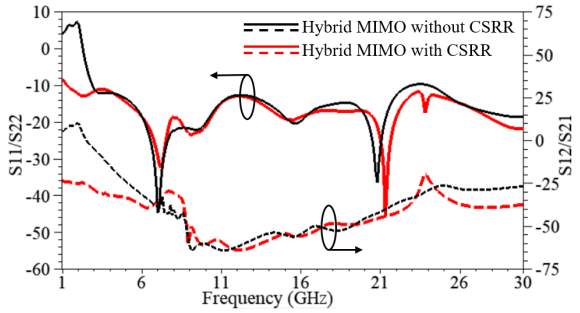

FIGURE 5. Comparison of reflection coefficient and isolation plot of proposed HFMA with and without CSRR.

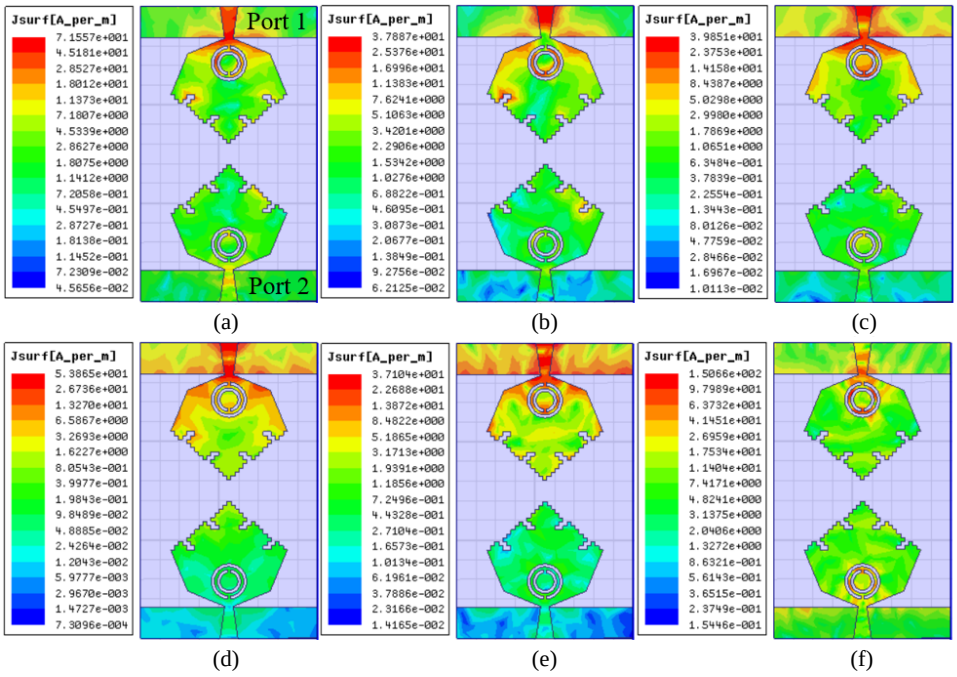

FIGURE 6. Surface current distribution of CSRR loaded HFMA (a) 2.3, (b) 7.2, (c) 9.10, (d) 15.50, (e) 21.30 and (f) 23.80 GHz frequency points.

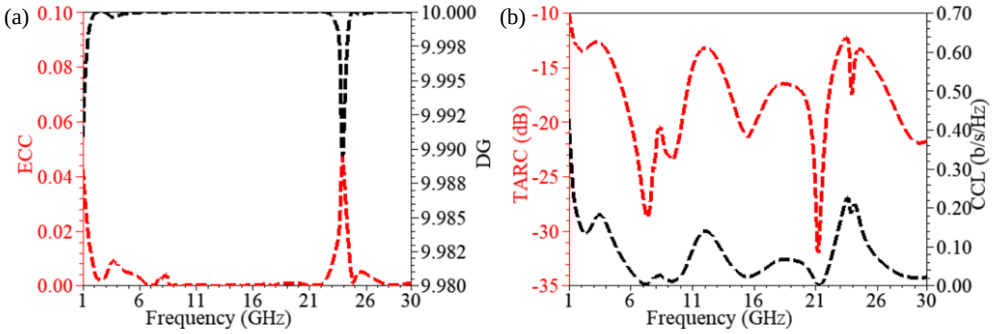

FIGURE 7. Diversity parameters of CSRR loaded HFMA; (a) envelope correlation coefficient (ECC) and diversity gain (DG), (b) total active reflection coefficient (TARC) and channel capacity loss (CCL).

concentration of solid current along with the tapered feed line, which leads to an increase in impedance bandwidth and a reduction in mutual coupling between the excitation ports. Because of the CSRR loading, as illustrated in Fig. 6, decreasing the mutual coupling in the ports results in better isolation characteristics.

6. DIFFERENT DIVERSITY PARAMETERS OF THE PROPOSED HFMA

1. ECC: ECC investigates the coupling between nearby antenna elements. In ideal circumstances, the ECC value should be zero, but for nearby uncorrelated antennas, the ECC value should be less than 0.5. The value of ECC obtained using S parameters in Equation (4) [24] and representation of the ECC is graphically depicted in Fig. 7(a). It reveals ECC value less than 0.05 for the operative frequency range.

$$\mathrm{ECC} = \frac{\left|S_{11}^{*}S_{12} + S_{21}^{*}S_{22}\right|^{2}}{\left(1-\left(\left|S_{11}\right|^{2}+\left|S_{21}\right|^{2}\right)\right)\left(1-\left(\left|S_{22}\right|^{2}+\left|S_{12}\right|^{2}\right)\right)} \quad (4)$$

2. Diversity Gain: MIMO performance can also be assessed by the diversity gain of an antenna. To achieve acceptable quality DG value must be close to 10 dB. The DG for the proposed HFMA is evaluated using Equation (5).

$$\mathrm{DG} = 10 \times \sqrt{1 - |\mathrm{ECC}|} \quad (5)$$

The plot of DG is shown in Fig. 7(a), from which DG value is approximately 10 dB throughout the operative frequency range [25].

3. TARC: TARC stands for total incident power divided by total reflected power in a multiport antenna system, is defined to provide a more accurate description of MIMO systems for designed HFMA and is evaluated using Equations (6) and (7). The

TABLE 5. Comparison of the proposed HFMA with existing literature.

Reference	No. of Ports	Bandwidth (GHz)	Antenna dimensions (mm^3)	Isolation (dB)	ECC (dB)	Peak Gain (dBi)
[24]	4	10.5	$72 \times 72 \times 0.8$	> 18	< 0.06	6
[25]	4	6.7	$32 \times 15 \times 32$	> 15	< 0.4	5.41
[26]	2	11.7	$12 \times 25.4 \times 0.8$	-	< 0.005	6–8
[27]	4	13	$58 \times 58 \times 0.8$	> 18	< 0.07	7
[28]	2	0.07	$26 \times 13.75 \times 1.6$	> 20	-	-
[29]	2	3	$40 \times 20 \times 1.6$	-84.62		5.8
[30]	4	0.14	$100 \times 50 \times 0.8$	-	-	-
[31]	4	3.40–3.625(0.225) 3.90–4.55(0.65)	$80 \times 70 \times 0.8$	> 20.1	< 0.3	6.5
[32]	2	0.15	$50 \times 50 \times 0.8$	-17.3	< 0.5	0.2148
[33]	4	0.42	$100 \times 50 \times 0.8$	> 10	-	0.8
This work	2	28.72	$75 \times 45 \times 1.6$	-55.86	0.05	20.89

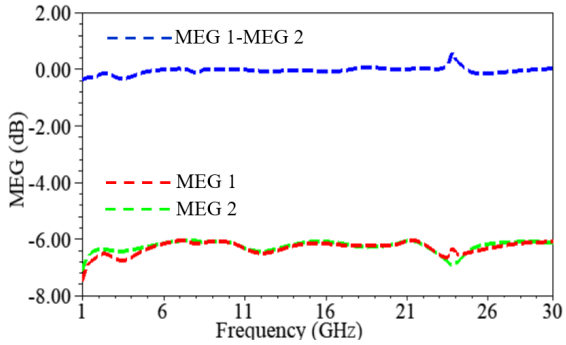

FIGURE 8. Mean Effective Gain (MEG) of CSRR loaded proposed HFMA between ports (1, 2).

simulated TARC against frequency plot is shown in Fig. 7(b).

$$\Gamma_a^t = \frac{\sqrt{\sum_{i=1}^{N} |b_i|^2}}{\sqrt{\sum_{i=1}^{N} |a_i|^2}} \tag{6}$$

$$\Gamma_a^t = \frac{\sqrt{\left(\left|\left(S_{11} + S_{12}^{e^{j\theta}}\right)\right|^2 + \left|\left(S_{21} + S_{22}^{e^{j\theta}}\right)\right|^2\right)}}{\sqrt{2}} \tag{7}$$

where $b_i = [S] \cdot a_i \cdot [S]$ is the scattering matrix, $[b] \rightarrow$ scattering vector, and $[a] \rightarrow$ excitation vector.

4. CCL: The CCL of the MIMO antenna provides details of channel capacity reduction due to the correlation effect. The CCL of the proposed HFMA was evaluated using equations in [8, 9]. Less than 0.4 bits per second/Hz is the perfect recognized CCL. Fig. 7(b) shows the CCL against frequency simulation results, which were smaller than the expected extreme value of 0.4 bits/sec/Hz.

$$C_{\text{loss}} = -\log_2 \left|\beta^R\right| \tag{8}$$

$$\beta^R = \begin{bmatrix} \beta_{11} & \beta_{12} \\ \beta_{21} & \beta_{22} \end{bmatrix} \tag{9}$$

where

$$\beta_{11} = 1 - \left(|S_{11}|^2 + |S_{12}|^2\right)$$

$$\beta_{22} = 1 - \left(|S_{22}|^2 + |S_{21}|^2\right)$$

$$\beta_{12} = -\left(S_{11}^* S_{12} + S_{21}^* S_{22}\right)$$

$$\beta_{21} = -\left(S_{22}^* S_{21} + S_{12}^* S_{11}\right)$$

5. MEG: The optimal MEG value falls precisely between ± 3 dB, and it is the ratio of mean received power to mean incident power. To improve MIMO antenna performance, the ratio of MEG must adhere to the requirements $|\text{MEG}_i/\text{MEG}_j| < \pm 3$ dB [27], where i and j indicate antenna elements 1 and 2. Equations (10) and (11) have been utilized for evaluating MEG as depicted in Fig. 8.

$$\text{MEG}_i = 0.5\left[1 - |S_{ii}|^2 - |S_{ij}|^2\right] \tag{10}$$

$$\text{MEG}_j = 0.5\left[1 - |S_{ij}|^2 - |S_{jj}|^2\right] \tag{11}$$

7. FABRICATED PROTOTYPE AND RESULTS

The final prototype of the designed HFMA is fabricated as depicted in Fig. 9. Fig. 10 compares simulated and fabricated values of the S-parameters of the proposed HFMA and finds a strong correlation between them, but a few inconsistencies may arise because of fabrication problems, environmental conditions, or reflection on the SMA connector. The suggested HFMA exhibits a wider bandwidth of 28.72 GHz from 1.28 to 30 GHz (for $S_{11} \leq -10$ dB). Additionally, the maximum port isolation of -55.86 dB of the proposed antenna is obtained. Further, simulated and fabricated 2D radiation patterns at different resonant frequencies including 2.3, 7.2, 9.10, 15.50, 21.30, and 23.80 GHz are shown in Fig. 11. Almost omnidirectional radiation patterns are produced by the proposed antenna in both planes.

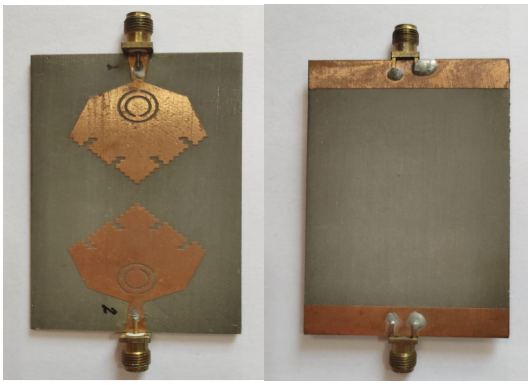

FIGURE 9. Front and back view of fabricated CSRR loaded HFMA.

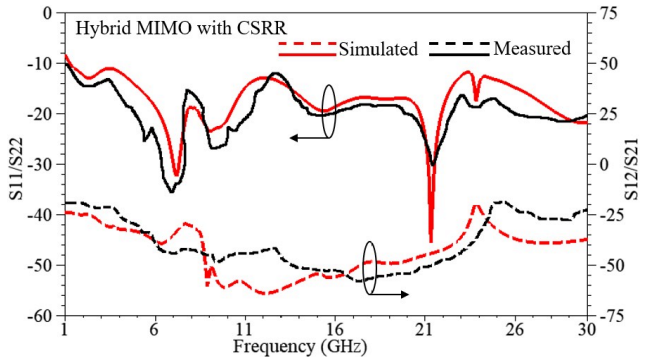

FIGURE 10. Simulated and measured S-parameter analysis of proposed HFMA.

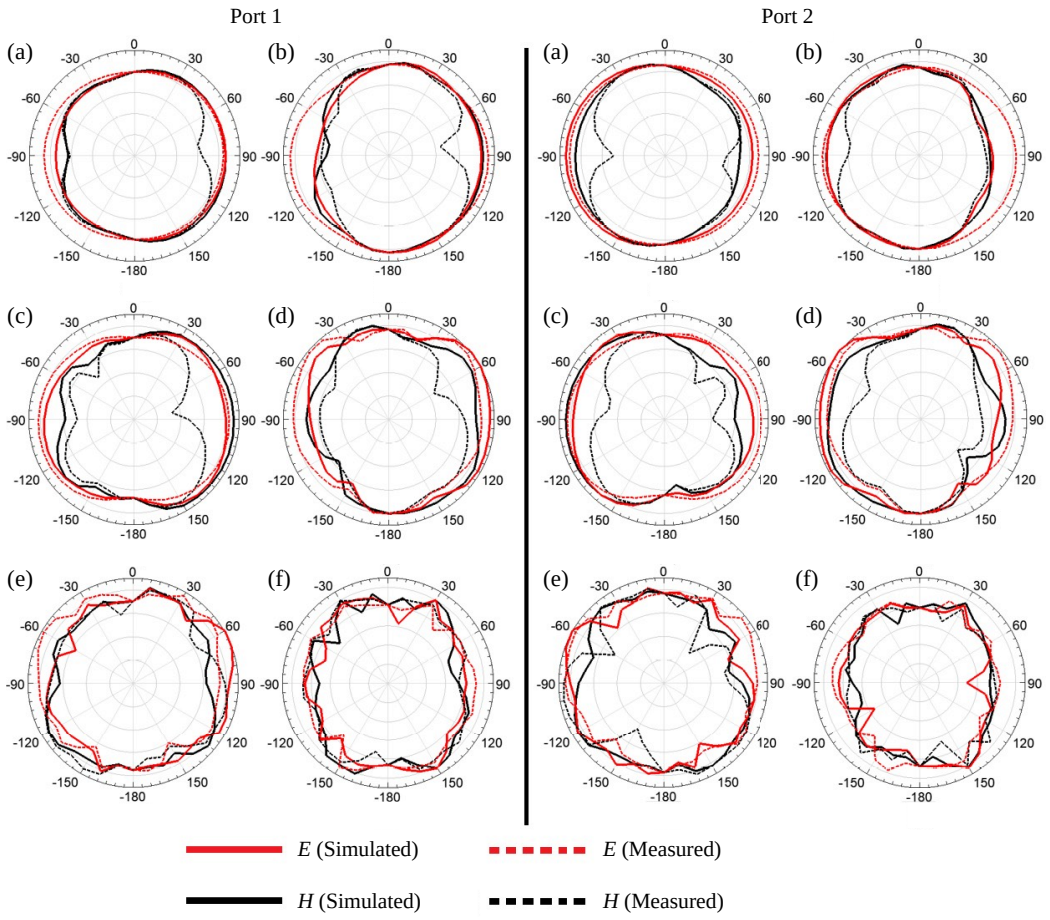

FIGURE 11. Simulated and measured radiation patterns of proposed CSRR loaded HFMA at (a) 2.3, (b) 7.2, (c) 9.10, (d) 15.50, (e) 21.30 and (f) 23.80 GHz frequency points in both E (XZ-plane) and H (YZ-plane).

However, at higher frequencies, patterns exhibit slight distortion, which might be attributed to differentiating short wavelength current on the antenna assembly.

After loading CSRR, the suggested antenna becomes more directive over the entire frequency range, as shown by the peak realization gain plot for the suggested CSRR-loaded HFMA, which is compared and shown in Fig. 12. These two outcomes agree fairly well with one another, with some differences attributed to antenna design characteristics such as environmental characteristics and physical characteristics.

The proposed HFMA with CSRR was also contrasted with other already existing MIMO antennas. From comparative Table 5, it is evident that the proposed HFMA demonstrates exceptional performance with an isolation of -55.86 dB, a wide bandwidth of 28.72 GHz, a peak realized gain of 21 dBi, and ECC less than 0.05. So the proposed HFMA shows better performance parameters than other antennas presented in the literature.

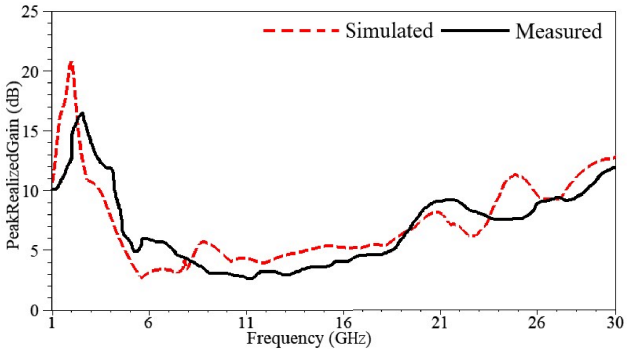

FIGURE 12. Peak realized gain versus frequency plot of proposed HFMA.

8. CONCLUSION

This article presents the design of a two-port HFMA with CSRR loading for 5G and other wireless applications, spanning the 1–30 GHz frequency range. A defective ground plane and CSRR are incorporated to enhance isolation, reduce mutual coupling, and improve the bandwidth, gain, and other parameters of the proposed HFMA. Comparative investigation shows that in terms of bandwidth, isolation, mutual coupling, and gain, the CSRR-loaded MIMO antenna performs significantly better than its counterpart without CSRR. The proposed HFMA exhibits a maximum isolation of −55.86 dB and a broader impedance bandwidth of 28.72 GHz (1.28 to 30.0 GHz). Additionally, various diversity parameters such as ECC, TARC, DG, MEG, CCL are achieved within acceptable limits. Although the proposed HFMA is optimized for 5G communication, its features make it highly suitable for a range of other advanced applications, including Internet of Things (IoT), satellite communications, and vehicular networks in the frequency range of 1–30 GHz band.

REFERENCES

[1] Najafy, V. and M. Bemani, "Mutual-coupling reduction in triple-band MIMO antennas for WLAN using CSRRs," *International Journal of Microwave and Wireless Technologies*, Vol. 12, No. 8, 762–768, 2020.

[2] Pallavi, H. V., A. P. J. Chandra, and Paramesha, "5G wireless communication microstrip patch antenna array design with MIMO," *Multimedia Tools and Applications*, Vol. 82, No. 20, 31 129–31 155, 2023.

[3] Dharmarajan, A., P. Kumar, and T. J. O. Afullo, "A high gain UWB human face shaped MIMO microstrip printed antenna with high isolation," *Multimedia Tools and Applications*, Vol. 81, No. 24, 34 849–34 862, 2022.

[4] Selvaraju, R., M. H. Jamaluddin, M. R. Kamarudin, J. Nasir, and M. H. Dahri, "Complementary split ring resonator for isolation enhancement in 5G communication antenna array," *Progress In Electromagnetics Research C*, Vol. 83, 217–228, 2018.

[5] Sahoo, M., A. Patani, and B. Makwana, "A review on dielectrical resonant antenna based on the performance of gain and bandwidth," *Multimedia Tools and Applications*, Vol. 82, No. 16, 24 645–24 679, 2023.

[6] Kumar, S., G. H. Lee, D. H. Kim, W. Mohyuddin, H. C. Choi, and K. W. Kim, "Multiple-input-multiple-output/diversity antenna with dual band-notched characteristics for ultra-wideband applications," *Microwave and Optical Technology Letters*, Vol. 62, No. 1, 336–345, 2020.

[7] Sun, J.-S., H.-S. Fang, P.-Y. Lin, and C.-S. Chuang, "Triple-band MIMO antenna for mobile wireless applications," *IEEE Antennas and Wireless Propagation Letters*, Vol. 15, 500–503, 2015.

[8] Lee, J.-Y., S.-H. Kim, and J.-H. Jang, "Reduction of mutual coupling in planar multiple antenna by using 1-D EBG and SRR structures," *IEEE Transactions on Antennas and Propagation*, Vol. 63, No. 9, 4194–4198, 2015.

[9] Sharawi, M. S., M. U. Khan, A. B. Numan, and D. N. Aloi, "A CSRR loaded MIMO antenna system for ISM band operation," *IEEE Transactions on Antennas and Propagation*, Vol. 61, No. 8, 4265–4274, 2013.

[10] Kaur, M. and J. S. Sivia, "Giuseppe peano and cantor set fractals based miniaturized hybrid fractal antenna for biomedical applications using artificial neural network and firefly algorithm," *International Journal of RF and Microwave Computer-Aided Engineering*, Vol. 30, No. 1, e22000, 2019.

[11] Bangi, I. S. and J. S. Sivia, "Minkowski and Hilbert curves based hybrid fractal antenna for wireless applications," *AEU — International Journal of Electronics and Communications*, Vol. 85, 159–168, 2018.

[12] Bhatia, S. S. and J. S. Sivia, "On the design of fractal antenna array for multiband applications," *Journal of the Institution of Engineers (India): Series B*, Vol. 100, 471–476, 2019.

[13] Sran, S. S. and J. S. Sivia, "PSO and IFS techniques for the design of wearable hybrid fractal antenna," *International Journal of Electronics*, Vol. 108, No. 12, 2039–2057, 2021.

[14] Sran, S. S. and J. S. Sivia, "Design of a novel wearable hybrid fractal antenna for Wi-Fi, Bluetooth, and WiMax applications," *Wireless Personal Communications*, Vol. 132, No. 1, 737–755, 2023.

[15] Bharti, G. and J. S. Sivia, "A design of compact wideband antenna based on hybridization of Minkowski fractal curves on hexagonal patch and partial ground plane with truncated corners," *Wireless Personal Communications*, Vol. 124, No. 2, 1609–1621, 2022.

[16] Kaur, M. and J. S. Sivia, "Artificial bee colony algorithm based modified circular-shaped compact hybrid fractal antenna for industrial, scientific, and medical band applications," *International Journal of RF and Microwave Computer-Aided Engineering*, Vol. 32, No. 3, e22994, 2022.

[17] Kakkar, S., T. S. Kamal, and A. P. Singh, "On the design and analysis of I-shaped fractal antenna for emergency management," *IETE Journal of Research*, Vol. 65, No. 1, 104–113, 2019.

[18] Kaur, M., J. S. Sivia, and N. Kaur, "Symmetric circular-shaped multiband hybrid fractal antenna using TLBO approach: Design and measurement," *International Journal of Electronics*, Vol. 109, No. 8, 1443–1460, 2022.

[19] Khalifa, M. O., A. M. Yacoub, and D. N. Aloi, "Compact 2×2 and 4×4 MIMO antenna systems for 5G automotive applications," *The Applied Computational Electromagnetics Society Journal (ACES)*, Vol. 36, No. 6, 762–778, 2021.

[20] Goyal, R. K. and U. S. Modani, "A compact MIMO microsrip patch antenna design at 28 GHz for 5G smart phones," *International Journal of Engineering Research & Technology*, Vol. 9, No. 4, 1–4, 2021.

[21] Singh, C. and P. C. K. Raja, "Hybrid optimization assisted transmit antenna selection for massive MIMO technology," *Multimedia Tools and Applications*, Vol. 83, No. 7, 20 909–20 929, 2024.

[22] Alkaraki, S. and Y. Gao, "2×2 and 4×4 MIMO antennas for 5G mm-Wave wireless communication," in *2019 IEEE International*

Symposium on Antennas and Propagation and USNC-URSI Radio Science Meeting, 1419–1420, Atlanta, GA, USA, 2019.

[23] Riaz, M. J., A. Sultan, M. Zahid, A. Javed, Y. Amin, and J. Loo, "MIMO antennas for future 5G communications," in *2020 IEEE 23rd International Multitopic Conference (INMIC)*, 1–4, Bahawalpur, Pakistan, Nov. 2020.

[24] Kumar, S., G. H. Lee, D. H. Kim, W. Mohyuddin, H. C. Choi, and K. W. Kim, "Multiple-input-multiple-output/diversity antenna with dual band-notched characteristics for ultra-wideband applications," *Microwave and Optical Technology Letters*, Vol. 62, No. 1, 336–345, 2020.

[25] Saravanan, M., R. Kalidoss, B. Partibane, and K. S. Vishvaksenan, "Design of an interlocked four-port MIMO antenna for UWB automotive communications," *International Journal of Microwave and Wireless Technologies*, Vol. 14, No. 2, 239–246, 2022.

[26] Venkateswara Rao, M., B. T. P. Madhav, J. Krishna, Y. U. Devi, T. Anilkumar, and B. P. Nadh, "CSRR-loaded T-shaped MIMO antenna for 5G cellular networks and vehicular communications," *International Journal of RF and Microwave Computer-Aided Engineering*, Vol. 29, No. 8, e21799, 2019.

[27] Kumar, P., S. Urooj, and F. Alrowais, "Design and implementation of quad-port MIMO antenna with dual-band elimination characteristics for ultra-wideband applications," *Applied Sciences*, Vol. 10, No. 5, 1715, 2020.

[28] Van Yem, V., P. V. Chi, and B. Journet, "Novel MIMO antenna using complementary split ring resonator (CSRR) for LTE applications," in *The 2012 International Conference on Advanced Technologies for Communications*, 222–226, Ha Noi, Vietnam, 2012.

[29] Kumar, S. and A. S. Dixit, "A miniaturized CSRR loaded 2-element MIMO antenna for LTE band," *Mathematical Modelling of Engineering Problems*, Vol. 8, No. 6, 984, 2021.

[30] Satishkumar, M. V., T. Gunasekaran, S. A. S. A. Ismaili, and S. Balambigai, "MIMO-CSRR antenna for ISM band applications," *Wireless Personal Communications*, 2021.

[31] Jha, P., A. Kumar, A. De, and R. K. Jain, "Modified CSRR based dual-band four-element MIMO antenna for 5G smartphone communication," *Progress In Electromagnetics Research Letters*, Vol. 101, 35–42, 2021.

[32] Malathi, C. J. and D. Thiripurasundari, "CSRR loaded 2×1 triangular MIMO antenna for LTE band operation," *Advanced Electromagnetics*, Vol. 6, No. 3, 78–83, 2017.

[33] Sharawi, M. S., M. U. Khan, A. B. Numan, and D. N. Aloi, "A CSRR loaded MIMO antenna system for ISM band operation," *IEEE Transactions on Antennas and Propagation*, Vol. 61, No. 8, 4265–4274, 2013.